Overlapping spin synchrotron sideband resonances

S. Y. Lee and M. Berglund*
Department of Physics, Indiana University, Bloomington, Indiana 47405
(Received 20 March 1996)

The synchrotron sideband spin resonances are shown to arise from the kinematic effect of spin phase modulation with resonance strengths proportional to that of the primary spin resonance. We develop a method to analyze overlapping spin resonances and apply it to fit polarization data of SPEAR and data recently obtained from polarized beam experiments at the IUCF cooler ring. The implication of our analyses is that synchrotron sidebands can only be corrected by correcting its principle resonance. Furthermore, the effect of synchrotron sidebands in proton synchrotrons is to change the resonance phase without affecting the magnitude of the strength. [S1063-651X(96)04907-0]

PACS number(s): 29.27.Bd, 41.75.−i, 03.20.+i, 05.45.+b

I. INTRODUCTION

The study of the proton spin structure function has become an important topic in high energy physics experiments, which require acceleration and storage of polarized protons in synchrotrons. However, many depolarizing spin resonances may be encountered when accelerating a polarized beam. Thus understanding spin dynamics for polarized beams in synchrotrons is an important topic in accelerator physics.

The spin equation of motion, governed by the magnetic interaction between the magnetic dipole moment of the particle and the electro-magnetic fields of synchrotrons, is given by the Thomas-Bargmann-Michel-Telegdi (BMT) equation [1]

$$\frac{d\vec{S}}{dt}=\frac{e}{\gamma m}\vec{S}\times\left[(1+G\gamma)\vec{B}_{\perp}+(1+G)\vec{B}_{\parallel}+\left(G\gamma+\frac{\gamma}{\gamma+1}\right)\frac{\vec{E}\times\vec{\beta}}{c}\right], \quad (1)$$

where $G=g/2-1$ is the anomalous magnetic g factor, γ is the relativistic Lorentz factor, $\vec{B}_{\perp}$ and $\vec{B}_{\parallel}$ are the transverse and longitudinal components of the magnetic field with respect to the velocity vector $\vec{\beta}$, and $\vec{E}$ is the electric field. Hereafter, we will neglect the electric field contribution. For synchrotrons with planar geometry, vertical magnetic fields are needed to guide the orbiting particle for a closed path. Taking the cyclotron frequency into account, the spin vector precesses about the vertical axis at a frequency of $G\gamma f_0$, where f_0 is the revolution frequency. The quantity $G\gamma$, representing the number of spin precession per revolution, is called the spin tune.

In synchrotrons, strong quadrupole fields are also needed to focus the beam to a small size. Those particles moving off center vertically in quadrupoles will experience horizontal fields, which can perturb the spin vector away from the vertical axis. Using the Thomas-BMT equation, the spin resonance strength is given by the Fourier amplitude of the spin perturbing fields in synchrotrons [2,3], i.e.,

$$\epsilon_K=\frac{1}{2\pi}\oint\left[(1+G\gamma)\frac{\Delta B_x}{B\rho}+(1+G)\frac{\Delta B_{\parallel}}{B\rho}\right]e^{iK\theta}ds, \quad (2)$$

where θ is the orbital bending angle, ΔB_x is the radial perturbing field, $\Delta B_{\parallel}$ is the longitudinal perturbing field, and $B\rho$ is the magnetic rigidity of the beam. In synchrotrons, there is little or no longitudinal field and the transverse radial field arises mainly from dipole rolls and the vertical displacement in quadrupoles. Neglecting the effect of dipole rolls, the radial perturbing field is given by

$$\Delta B_x=\frac{\partial B_z}{\partial x}z+\mathcal{M}, \quad (3)$$

where $\mathcal{M}$ stands for higher order multipoles. In general, the vertical displacement is given by [4]

$$z=z_{\rm co}+z_{\beta}+C_x x_{\beta}+\frac{\Delta p}{p}D_z, \quad (4)$$

where $z_{\rm co}, z_{\beta}$ are, respectively, the closed orbit and the betatron coordinate, $C_x x_{\beta}$ arises from linear betatron coupling, and D_z is the vertical dispersion function resulting from nonplanar accelerator geometry and/or linear betatron coupling. Substituting Eq. (4) into Eq. (2), $z_{\rm co}$ gives rise to imperfection resonances located at $K=$ integers, z_{β} produces intrinsic resonances at $K=nP\pm\nu_z$, where P is the superperiod of the machine and ν_z is the vertical betatron tune, x_{β} generates linear coupling spin resonances and the vertical dispersion function term can produce synchrotron sidebands located at $K=n\pm\nu_{\rm syn}$, where $\nu_{\rm syn}$ is the synchrotron tune. Including $\mathcal{M}$, the spin resonance tunes are generally given by

$$K=n+k\nu_z+l\nu_x+m\nu_{\rm syn}, \quad (5)$$

where k,l,m,n are integers.

*Permanent address: Alfvén Laboratory Division of Accelerator Technology, Royal Institute of Technology, 10044 Stockholm, Sweden.

Defining a two-component spinor Ψ with $\vec{S}=\langle\Psi|\vec{\sigma}|\Psi\rangle$, the Thomas-BMT equation can be casted into the spinor equation

$$\frac{d\Psi}{d\theta}=-\frac{i}{2}\begin{pmatrix} G\gamma & -\xi \\ -\xi^* & -G\gamma \end{pmatrix}\Psi, \tag{6}$$

where ξ can be expanded in a Fourier series

$$\xi=\sum \epsilon_K e^{-iK\theta}. \tag{7}$$

Here ϵ_K is the resonance strength given by Eq. (2). If spin resonances do not overlap with each other so that the spin motion is under the influence of at most one harmonic in ξ, the spinor equation can be solved analytically [2,3].

However, overlapping resonances occur often in high energy accelerators. Numerically integrating the spinor equation, we find that overlapping spin resonances can sometimes be expressed as a single resonance with an effective resonance strength attainable from a linear combination of all spin resonances [3]. In high energy storage rings which use snakes to overcome spin resonances, we find that the overlapping imperfection and intrinsic resonances also produce even order snake resonances and generate spin tune shift so that each snake resonance (both odd and even order) split into two [5,6].

Indeed, polarized beam experiments showed that overlapping synchrotron sideband resonances were important in electron storage rings [7]. Similarly, overlapping synchrotron sideband resonances were found to be important at the Indiana University Cyclotron Facility (IUCF) cooler ring [9–12]. Why were overlapping synchrotron sidebands not observed in the polarized proton acceleration at the alternating-gradient synchroton (AGS) [8]? How do synchrotron sidebands arise? What happens when all synchrotron sidebands overlap with the principle resonance?

This paper examines the physics of synchrotron sideband spin resonances and analyze the existing data in terms of an overlapping resonance model. Section II examines the origin of synchrotron sideband spin resonances, Sec. III reviews the effect of overlapping resonances on spin motion. Section IV analyzes some experimental data. The conclusion is given in Sec. V.

II. SYNCHROTRON SIDEBAND RESONANCES

It is tempting to attribute the synchrotron sidebands to the vertical dispersion function term in Eq. (4), where the momentum deviation $\Delta p/p$ for an off-momentum particle is given by

$$\frac{\Delta p}{p}=\hat{a}\cos\nu_{\rm syn}\theta. \tag{8}$$

Here $\hat{a}$ is the amplitude of synchrotron oscillations. Indeed, the term $D_z(\Delta p/p)$ can produce first order synchrotron sidebands, located at $K=n\pm\nu_{\rm syn}$, around imperfection resonances. Because the resonance strength is proportional to the product of the synchrotron amplitude $\hat{a}$ and the vertical dispersion D_z, it would be too small to fit any experimental data. Note particularly that the dispersion function *cannot* generate synchrotron sidebands around intrinsic depolarization resonances.

Since the spin resonance driving term $(1+G\gamma)\Delta B_x/B\rho$ from the transverse error fields, depends only weakly on $\Delta p/p_0$ at high energy, the resonance strength is nearly independent of the momentum deviation of the particle. In other words, the resonance strength at synchrotron sidebands due to the transverse perturbing fields is small. In particular, there are no synchrotron sidebands around intrinsic resonances. Although the longitudinal perturbing fields can produce synchrotron sidebands, longitudinal fields are usually weak in synchrotrons. A possible mechanism to generate synchrotron sidebands around intrinsic resonance is the feed down from higher order multipoles. This effect is again very small.

So far, we conclude that the resonance strengths of synchrotron sidebands induced by the vertical dispersion function are small and there are no synchrotron sidebands around intrinsic resonances. However, synchrotron sidebands were observed to be very important in the Stanford Positron Electron Accelerator Ring (SPEAR) polarization data [7]. What is the mechanism for synchrotron sidebands? In the following, we will show that the enhancement of synchrotron resonances arises mainly from the kinematic effect.

We consider the spin equation of motion for a single primary spin resonance

$$\frac{d\Psi}{d\theta}=-\frac{i}{2}\begin{pmatrix} G\gamma & -\epsilon_K e^{-iK\theta} \\ -\epsilon_K^* e^{iK\theta} & -G\gamma \end{pmatrix}\Psi, \tag{9}$$

where K is the resonance tune and ϵ_K is the resonance strength. For an off-momentum particle with *linear* synchrotron motion given by Eq. (8), the spin tune is given by $G\gamma=G\gamma_0(1+\beta^2\Delta p/p_0)$, where $\gamma_0 mc^2$ is the energy of the synchronous particle. Now, we transform the spinor wave function into the spin precessing frame with

$$\Psi=e^{-i/2\int_0^\theta G\gamma d\theta\sigma_3}\Psi_I, \tag{10}$$

and obtain

$$\frac{d\Psi_I}{d\theta}=\frac{i}{2}\begin{pmatrix} 0 & \epsilon_K e^{-i(K\theta-\int G\gamma d\theta)} \\ \epsilon_K^* e^{i(K\theta-\int G\gamma d\theta)} & 0 \end{pmatrix}\Psi_I. \tag{11}$$

Using Eq. (8), the spin precessing phase for an off-momentum particle becomes

$$\int_0^\theta G\gamma d\theta=G\gamma_0\theta+\frac{\beta^2 G\gamma_0}{\nu_{\rm syn}}\hat{a}\sin\nu_{\rm syn}\theta. \tag{12}$$

In particular, we note that the spin precessing phase has been greatly enhanced by the smallness of the synchrotron tune. The effective spin phase modulation amplitude is $g=(\beta^2 G\gamma_0/\nu_{\rm syn})\hat{a}$.

TABLE I. Effective strengths for synchrotron sidebands.

Resonances	K	$K\pm\nu_{\rm syn}$	$K\pm 2\nu_{\rm syn}$	$K\pm 3\nu_{\rm syn}$
Effective strength	ϵ_K	$\frac{1}{2}g\epsilon_K$	$\frac{1}{8}g^2\epsilon_K$	$\frac{1}{48}g^3\epsilon_K$

Expanding the spin precessing phase in Fourier harmonics, the effective resonance driving term in the spinor equation becomes

$$\epsilon_K e^{-i(K\theta-\int G\gamma d\theta)}=\sum_{-\infty}^{\infty}\epsilon_K J_m(g)e^{-i(K-G\gamma_0-m\nu_{\rm syn})\theta}. \tag{13}$$

If the condition $|\epsilon_K J_m(g)|<\nu_{\rm syn}$ is satisfied, each synchrotron sideband behaves as an isolated resonance with resonance strength $\epsilon_K J_m(g)$, where $m=0,\pm1,\pm2,\ldots$, i.e., the off-momentum particle experiences spin resonances at *all* synchrotron sidebands. Using the small argument expansion for Bessel functions, Table I lists effective resonance strengths for synchrotron sidebands.

The physics of synchrotron sidebands can be understood as follows. The spin phase modulation due to a linear synchrotron motion can generate many sidebands around the spin tune. If one of the sidebands falls on the principle resonance, the spin is strongly perturbed. Thus the resonance strength of synchrotron sidebands is proportional to the strength of the principle resonance. Because the synchrotron tune is relatively small so that the particle stays at the spin resonance condition for a long time, the effect of the spin resonance is particularly enhanced.

For electron storage rings, the synchrotron tune is usually of the order 0.1, thus synchrotron sidebands may be well separated. The single resonance dominant model used above is applicable. There are many experimental data which have confirmed the enhanced synchrotron sideband resonances [7].

For proton synchrotrons, synchrotron tunes are normally about 10^{-3}, the enhancement factor can be large. This means that all synchrotron sidebands overlap with the principle resonance, and the single resonance dominant analysis used above is not valid anymore. In this case, we will show, in Sec. III, that the magnitude of the effective resonance strength by combining all synchrotron sidebands is equal to that of the principle resonance.

III. EFFECT OF OVERLAPPING RESONANCES

We consider a simple model of overlapping resonances with

$$\xi=\epsilon_1 e^{-iK_1\theta}+\epsilon_2 e^{-iK_2\theta}, \tag{14}$$

where ϵ_1,ϵ_2 and K_1,K_2 are resonance strengths and resonance tunes, respectively. Let $\Delta=K_2-K_1$ be the spacing of these two spin resonances. We can classify multiple resonances into three categories:

(1) Isolated resonance with $|\Delta|\gg\max(\epsilon_1,\epsilon_2)$,

(2) Overlapping resonances with $|\Delta|\ll\min(\epsilon_1,\epsilon_2)$,

(3) Nearly overlapping resonances with $|\Delta|\geqslant\max(\epsilon_1,\epsilon_2)$.

The first case has been extensively studied in Ref. [2,3]. In this section, we will examine the latter two cases.

A. Overlapping resonances

When K_1 and K_2 are nearly equal, two harmonics in ξ can be combined to be

$$\xi=A(\epsilon_1,\epsilon_2,|\Delta|\theta)e^{-i\overline{K}\theta}, \tag{15}$$

where $\overline{K}=(K_1+K_2)/2$, $\Delta=K_2-K_1$, and A is a slowly modulating amplitude function. To study the physics of overlapping resonances, the spinor equation is solved numerically with a uniform acceleration rate through these resonances.

Let $G\gamma=\kappa_0+\alpha\theta$, where $\alpha=dG\gamma/d\theta$ is the constant acceleration rate. Let θ_0 be the orbital angle where the spin tune of the particle is equal to the spin resonance tune, i.e.,

$$G\gamma=\kappa_0+\alpha\theta_0=\overline{K}.$$

Now we define an asymptotic orbiting angle θ_a such that $\alpha\theta_a=3\times\max(\epsilon_1,\epsilon_2)$, so that when the orbiting angle satisfy $|\theta-\theta_0|>\theta_a$, the spinor wave function is in the asymptotic region and the spin resonance has little effect on spin motion. The factor of 3 for the asymptotic region has been derived from numerical simulations and analytic solution of a single resonance model [3].

In general, the effective resonance strength experienced by the polarized beam is the integrated effect of the effective amplitude A. However, if the condition $|\Delta|\theta_a\ll1$ is fulfilled, the effective resonance strength is simply given by

$$\epsilon_{\rm eff}=A(\epsilon_1,\epsilon_2,|\Delta|[\theta_0+(\theta-\theta_0)])\approx A(\epsilon_1,\epsilon_2,|\Delta|\theta_0), \tag{16}$$

which is time independent. The polarization after passing through these two overlapping resonances is given by the Froissart-Stora formula [13]

$$\frac{P_f}{P_i}=2e^{-\pi|\epsilon_{\rm eff}|^2/2\alpha}-1. \tag{17}$$

This means that two overlapping resonances may be replaced by a single resonance with an effective resonance strength given by Eq. (16).

To verify the model, the spinor equation has been numerically integrated with a simplified two resonance model [3]

$$\xi=\epsilon e^{-iK_1\theta}+\epsilon e^{-i(K_1+\Delta)\theta}$$

with $K_1=3.2$, $\overline{K}=3.2+(\Delta/2)$, $\alpha=4.86\times10^{-5}$. The effective resonance strength for this simplified model is

$$\epsilon_{\rm eff}=2\epsilon\cos\left[\frac{\Delta}{2}\theta_0+\frac{\Delta}{2}(\theta-\theta_0)\right]. \tag{18}$$

Furthermore, if two nearby spin resonances satisfies $\Delta/2\ \theta_a\ll1$, the effective spin resonance strength becomes

$$\epsilon_{\rm eff}=2\epsilon\cos\left(\frac{\Delta}{2}\theta_0\right), \tag{19}$$

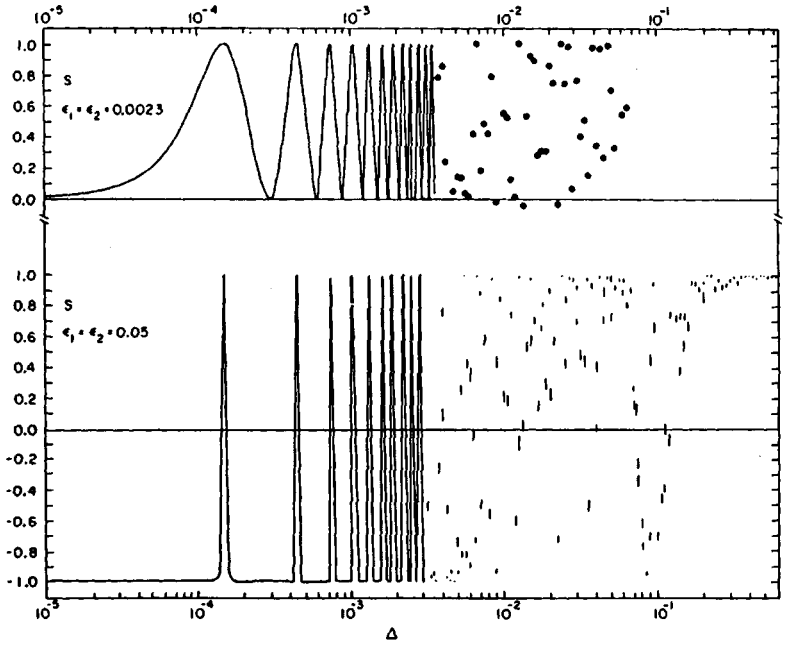

FIG. 1. The vertical polarization obtained from solving the spinor equation with two nearby resonance at $K_1=3.2$ and $K_2=K_1+\Delta$ as a function of the spacing parameter Δ. The resonance strengths are $\epsilon_1=\epsilon_2=0.0023$ for the upper plot and 0.05 for the lower plot. Note here that if $|\Delta|\leqslant 3\times 10^{-3}$, these two resonances can be combined into one resonance with effective strength obtained from linear superposition.

which is independent of time. The final polarization becomes

$$S(\Delta)=2\exp\left\{-\frac{2\pi|\epsilon|^2}{\alpha}\cos^2\left(\frac{\Delta}{2}\theta_0\right)\right\}-1. \tag{20}$$

The top plot of Fig. 1 taken from Ref. [3] shows the final polarization obtained from numerical solutions of the spinor equation as a function of Δ with $\epsilon=0.0023$, which was chosen such that a resonance strength 2ϵ would fully depolarize the beam. Cancelation of these two spin resonances occurs at

$$|\Delta|\theta_0=|\Delta|\frac{\overline{K-\kappa_0}}{\alpha}=(2m+1)\pi,\quad m=1,2,3,\ldots, \tag{21}$$

where $S(\Delta)=1$ was confirmed by numerical calculations up to $\Delta\leqslant 0.005$.

The lower plot shows similar results with $\epsilon=0.05$, where each individual resonance can cause a complete spin flip. In this case, Eq. (20) remains valid up to $\Delta\leqslant 0.002$. Because of very large resonance strength, the range of Δ in which these two resonances cancel each other becomes very narrow. It is also worth pointing out that the spin has flipped twice at $\Delta>0.3\approx 3(\epsilon_1+\epsilon_2)$ as shown in the lower plot. Thus the factor of 3 used in defining the asymptotic region is a reasonable approximation for polarized beam acceleration through a resonance.

Now we can discuss the effect of overlapping synchrotron sidebands in proton synchrotrons. When the spacing between two spin resonances is smaller than 10^{-3}, the effective spin resonance strength becomes the sum of all resonances. For synchrotron sidebands of proton synchrotrons, the effective resonance strength of Eq. (13) becomes

$$\epsilon_{\rm eff}\approx\epsilon_K\sum J_m(g)e^{im\nu_{\rm syn}\theta_0}=\epsilon_K e^{ig\sin\nu_{\rm syn}\theta_0}. \tag{22}$$

This means that the synchrotron motion changes merely the phase of the principle resonance strength without affecting its magnitude.

B. Nearly overlapping resonances

In the nearly overlapping resonance regime with $\Delta\geqslant$ max (ϵ_1,ϵ_2), the Froissart-Stora formula may not be applicable. This is evidently shown in Fig. 1 in the region $\Delta\in[0.01,0.3]$. We will analyze the two resonance model of Eq. (14) as follows:

Let us transform the spinor equation onto the resonance precession frame of K_1, i.e.,

$$\Psi_{K1}=e^{i\frac{1}{2}K_1\theta\sigma_3}\Psi \tag{23}$$

and obtain

$$\frac{d\Psi_{K1}}{d\theta}=\frac{i}{2}\lambda_1(\hat{\vec{n}}_1\cdot\vec{\sigma})\Psi_{K1}+\frac{i}{2}\begin{pmatrix}0 & \epsilon_2 e^{-i\Delta\theta}\\ \epsilon_2^* e^{i\Delta\theta} & 0\end{pmatrix}\Psi_{K1}, \tag{24}$$

where

$$\lambda_1=[\delta_1^2+|\epsilon_1|^2]^{1/2},\quad \delta_1=K_1-G\gamma,$$

$$\hat{\hat{n}}_1=\frac{1}{\lambda_1}(\delta_1\hat{\hat{e}}_z+\epsilon_{1r}\hat{\hat{e}}_x-\epsilon_{1i}\hat{\hat{e}}_s),$$

$$\epsilon_1=\epsilon_{1r}+i\epsilon_{1i}.$$

Here $\hat{\hat{e}}_x$, $\hat{\hat{e}}_s$, and $\hat{\hat{e}}_z$ are base vectors for the particle coordinate in the Frenet-Serret coordinate system.

The first term of Eq. (24) describes the precession of any arbitrary polarization vector around the spin closed orbit $\hat{\hat{n}}_1$, which precesses around the vertical axis with the tune K_1. The second term describes the perturbation due to the nearby resonance K_2. If $|\delta_1+\Delta|\gg|\epsilon_2|$, then the reso-

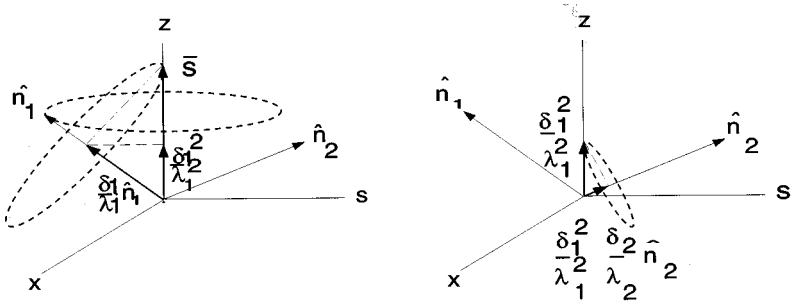

FIG. 2. Schematic drawing of spin closed orbits of nearly overlapping spin resonances. The left plot shows the survived spin vector in the presence of a spin resonance at K_1, and the right plot shows the effect of the spin resonance K_2 on the final polarization vector.

nance K_2 can be treated perturbatively. We however will discuss the situation when $\delta_1+\Delta\approx 0$ with $|\Delta|\geqslant \max(\epsilon_1,\epsilon_2)$.

Now we transform the spinor into the spin precession frame of K_1 with

$$\tilde{\Psi}_{K1}=e^{-(i/2)\lambda_1\theta\hat{\hat{n}}_1\cdot\vec{\sigma}}\Psi_{K1} \tag{25}$$

to obtain

$$\frac{d\tilde{\Psi}_{K1}}{d\theta}=e^{-(i/2)\lambda_1\theta\hat{\hat{n}}_1\cdot\vec{\sigma}}\left(\frac{i}{2}\right)e^{-\frac{i}{2}\Delta\theta\sigma_3}\times\begin{pmatrix}0 & \epsilon_2\\ \epsilon_2^* & 0\end{pmatrix}e^{(i/2)\Delta\theta\sigma_3}e^{(i/2)\lambda_1\theta\hat{\hat{n}}_1\cdot\vec{\sigma}}\tilde{\Psi}_{K1}. \tag{26}$$

If $|\delta_1|\approx|\Delta|>|\epsilon_1|$, we transform the spinor into the K_2 resonance frame with

$$\Psi_{K2}=e^{(i/2)\delta_2\theta\sigma_3}\tilde{\Psi}_{K1},$$

where $\delta_2=K_2-G\gamma$, and obtain an approximation to Eq. (26) with

$$\frac{d\Psi_{K2}}{d\theta}\approx\frac{i}{2}\lambda_2(\hat{\hat{n}}_2\cdot\vec{\sigma})\Psi_{K2}, \tag{27}$$

where $\lambda_2=[\delta_2^2+|\epsilon_2|^2]^{1/2}$ is the spin precession tune around the spin closed orbit $\hat{\hat{n}}\hat{n}_2$ given by

$$\hat{\hat{n}}_2=\frac{1}{\lambda_2}(\delta_2\hat{\hat{e}}_z+\epsilon_{2r}\hat{\hat{e}}_x-\epsilon_{2i}\hat{\hat{e}}_s),$$

which precesses about the vertical axis at a tune K_2. Finally, the evolution of the spinor wave function from θ_0 to θ can be expressed as

$$\Psi(\theta)=e^{-(i/2)K_1\theta\sigma_3}e^{(i/2)\lambda_1\theta\hat{\hat{n}}_1\cdot\vec{\sigma}}\times e^{-(i/2)\delta_2\theta\sigma_3}e^{(i/2)\lambda_2(\theta-\theta_0)\hat{\hat{n}}_2\cdot\vec{\sigma}}e^{(i/2)\delta_2\theta\sigma_3}\times e^{-(i/2)\lambda_1\theta_0\hat{\hat{n}}_1\cdot\vec{\sigma}}e^{(i/2)K_1\theta_0\sigma_3}\Psi(\theta_0). \tag{28}$$

This series of precession frame transformation is schematically shown in Fig. 2. If the spacing between two spin resonances are larger than the resonance strengths (or widths), each resonance can be visualized as having a spin closed orbit precessing about the vertical axis with precession tunes K_1 and K_2, respectively. For a beam of polarized protons with vertical polarization injected into a storage ring, the polarization vector will precess about these spin closed orbits. We consider first the the resonance K_1, the survived polarization is given by

$$\vec{S}_{K1}=\frac{\delta_1}{\lambda_1}\hat{\hat{n}}_1, \tag{29}$$

which is schematically shown in the left plot of Fig. 2. Since $\hat{\hat{n}}_1$ precesses about the vertical axis with precession tune K_1, the polarization vector is given by

$$\vec{S}_{K1}=\frac{\delta_1}{\lambda_1}\left(\frac{|\epsilon_1|}{\lambda_1}\cos(K_1\theta+\chi_1),\frac{|\epsilon_1|}{\lambda_1}\sin(K_1\theta+\chi_1),\frac{\delta_1}{\lambda_1}\right),$$

where $\chi_1=\arctan(\epsilon_{1i}/\epsilon_{1r})$ is the phase of the resonance strength. If K_1 is not an integer, spin tune spread within the bunch will cause spin decoherence and the remaining polarization is the vertical component δ_1^2/λ_1^2.

Including the effect of the second resonance at K_2, the survived polarization is

$$\vec{S}_{K1K2}=\frac{\delta_1^2}{\lambda_1^2}\frac{\delta_2}{\lambda_2}\hat{\hat{n}}_2, \tag{30}$$

which is schematically shown in the right plot of Fig. 2. Now $\hat{\hat{n}}_2$ precesses about the vertical axis with precession tune K_2, the polarization vector becomes

$$\vec{S}_{K1K2}=\frac{\delta_1^2}{\lambda_1^2}\frac{\delta_2}{\lambda_2}\left(\frac{|\epsilon_2|}{\lambda_2}\cos(K_2\theta+\chi_2),\frac{|\epsilon_2|}{\lambda_2}\sin(K_2\theta+\chi_2),\frac{\delta_2}{\lambda_2}\right),$$

where $\chi_2=\arctan(\epsilon_{2i}/\epsilon_{2r})$.

Thus the vertical polarization of nearly overlapping spin resonances can be expressed as the product of the projection of each resonance, i.e.,

$$S_z=\prod_i\frac{\delta_i^2}{\lambda_i^2}, \tag{31}$$

and the radial polarization is given by

$$S_r=\sum_i\prod_{j\neq i}\frac{\delta_j^2}{\lambda_j^2}\frac{\delta_i|\epsilon_i|}{\lambda_i^2}\cos(K_i\theta+\chi_i). \tag{32}$$

The vertical and the horizontal polarization of the beam can then be obtained by *averaging* S_z and S_r over the particle distribution of the beam.

TABLE II. SPEAR machine parameters that fit the polarization data.

ν_x	ν_z	ν_s	ϵ_8	$\epsilon_{3+\nu_x}$	$\epsilon_{3+\nu_z}$	$\epsilon_{8+\nu_x-\nu_z}$
5.279 662	5.182 604	0.04 276	0.03	0.008	0.001	0.001

As the polarized beam travels along the ring, its polarization vector precesses about the vertical axis with a spin phase advance $K\theta$. Since θ advances by 2π every revolution, the radial polarization observed at one location in the ring will oscillate with a zero average if all resonance tunes K_i are not integers. On the other hand, if one of the resonances is an imperfection resonance, where K_i is an integer, the spin closed orbit is stationary and the radial polarization may not be zero.

IV. DATA FITTING

To verify the overlapping resonance model and the synchrotron sideband enhancement, we will analyze the well-known SPEAR data [7] and some synchrotron sideband data of the IUCF cooler ring [9–12].

A. SPEAR data

The first *systematic* study of spin resonances in a storage ring was the polarization data of SPEAR [7]. Many resonances were presented in Fig. 8 of Ref. [7], where one notes that there are

$$K=8, \quad 3+\nu_z, \quad 3+\nu_x$$

principle resonances with many synchrotron sidebands, and nonlinear resonances at $8+\nu_x-\nu_z, \nu_x+\nu_z-2$. The polarization data had been extensively studied by Chao [14], Mane [15], and Buon [16] with spin tracking programs.

Instead of repeating the spin tracking, we will use Eq. (31) of the weakly overlapping resonance model to fit the data and extract some relevant spin resonance information. Since synchrotron sidebands are particularly enhanced resulting from large spin chromaticity [17] and small synchrotron tune, the resonance strengths of synchrotron sidebands at $K\pm m\nu_{\rm syn}$ are given by $\epsilon_K J_m(g)$ with $g=\beta^2 G\gamma_0\hat{a}/\nu_{\rm syn}$, where $\hat{a}$ is the synchrotron amplitude. The number of free parameters are ϵ_8, $\epsilon_{3+\nu_x}$, $\epsilon_{3+\nu_z}$, and $\epsilon_{8+\nu_x-\nu_z}$, etc.

For an electron storage ring, the synchrotron amplitude is not a free parameter. The rms beam momentum spread for SPEAR at 3.6 GeV is given by

$$\sigma_{\Delta p/p}=\left(\frac{C_q}{J_E\rho}\right)^{1/2}\gamma\approx 8.7\times 10^{-4},$$

where the damping partition number is $J_E=2$, ρ is the bending radius, $C_q=3.84\times 10^{-13}$ m. If we choose $\hat{a}=\sqrt{6}\sigma_{\Delta p/p}$, we obtain $g=0.42$. Using Eq. (31) with the parameters listed in Table II, the solid line in Fig. 3 fits the synchrotron sidebands reasonably well, which are generated by its principle resonance with spin phase modulation. The resonance strength derived from the data fitting can be tested by Eq. (2) with the SPEAR lattice. Unfortunately, the process involves closed orbit error and linear betatron coupling, which may not be known with certainty.

B. Synchrotron sidebands near an imperfection resonance

Synchrotron sidebands around an imperfection resonance had also been observed in the snake experiments at the IUCF cooler ring [10]. Figure 4 shows the measured vertical and radial polarization vs the longitudinal field strength of the compensating solenoids at the IUCF cooler ring [10,11]. The vertically polarized protons at 104.5 MeV with 77% polarization were injected into the cooler ring and the radial and the vertical components of the beam polarization were measured as a function of the compensating solenoidal field at the cooling section [18]. The vertical polarization was found to be maximum at $B_\parallel L=0.0158$ T m, which corresponded to a fully compensated solenoidal field for spin motion.

The particle $G\gamma$ value for this experiment was 1.9925. Because of the horizontal orbit bump at the electron cooling section, the spin precession tune was shifted upward by about 0.0035 [11]. Thus the spin tune of the beam was $\nu_s=1.9960$. In the presence of the solenoidal field, the perturbed spin tune Q_s for an otherwise perfect synchrotron is given by

$$\cos\pi Q_s=\cos[\pi\nu_s]\cos\frac{\chi}{2}, \tag{33}$$

and the spin closed orbit vector $\hat{\vec{n}}_1=(n_{1x},n_{1s},n_{1z})$ is given by

$$n_{1x}=\frac{-1}{\sin\pi Q_s}\sin[\nu_s(\pi-\theta)]\sin\frac{\chi}{2}, \tag{34}$$

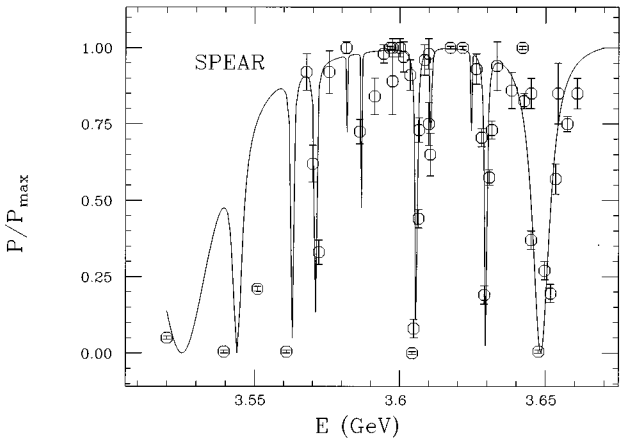

FIG. 3. The polarization of e^+ single beam in SPEAR is shown as a function of the beam energy [7]. The solid line is a fit to the eye by using a single resonance model with parameters: $\nu_x=5.279\,662, \nu_z=5.182\,604, \nu_s=0.042\,76$, $\sigma_\epsilon=8.7\times 10^{-4}$, and $\hat{a}=\sqrt{6}\sigma_\epsilon$.

$$n_{1s}=\frac{1}{\sin\pi Q_s}\cos[\nu_s(\pi-\theta)]\sin\frac{\chi}{2}, \tag{35}$$

$$n_{1z}=\frac{1}{\sin\pi Q_s}\sin[\pi\nu_s]\cos\frac{\chi}{2}, \tag{36}$$

where θ is the orbital angle between the observation point and the solenoid ($\theta=60°$ at the IUCF cooler ring), χ is the spin kick angle from the solenoid, i.e.,

$$\chi=(1+G)\frac{\Delta B_{\|}L}{B\rho},$$

where $\Delta B_{\|}L$ is the integrated solenoidal field error, and $B\rho$ is the beam rigidity. A larger spin precession angle χ will cause a larger deviation of the perturbed spin tune Q_s from an integer and the spin closed orbit also tilts further away from the vertical axis.

When a beam of vertically polarized protons is injected into the cooler, the polarization vector will precess about $\hat{\vec{n}}_1$. Thus the survived magnitude of polarization is $\vec{S}_{\rm inj}\cdot\hat{\vec{n}}_1=P_{\rm inj}n_{1z}$, and the final stable polarization vector is given by

$$\vec{P}_{\rm stable}=P_{\rm inj}n_{1z}(n_{1x}\hat{\vec{e}}_x+n_{1s}\hat{\vec{e}}_s+n_{1z}\hat{\vec{e}}_z. \tag{37}$$

Since ν_s is close to 2 and χ is small, the fractional part of the spin tune can be approximated by

$$Q_s\approx[(2-\nu_s)^2+\epsilon^2]^{1/2},\quad \epsilon=\frac{\chi}{2\pi}. \tag{38}$$

The final vertical and radial polarization is given by

$$S_v\approx P_{\rm inj}\frac{(2-\nu_s)^2}{(2-\nu_s)^2+\epsilon^2}, \tag{39}$$

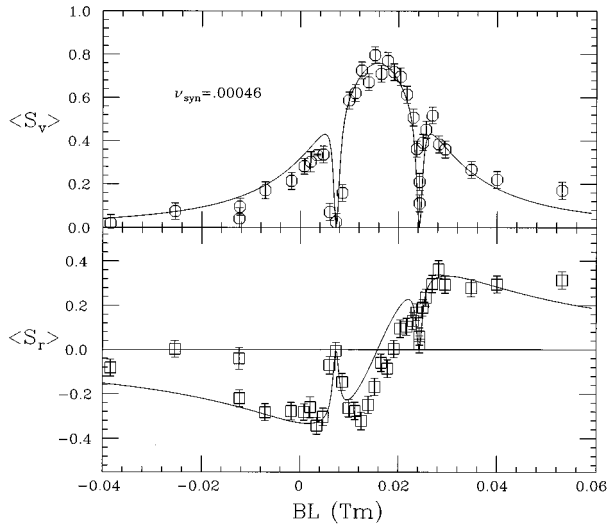

FIG. 4. The vertical and radial polarization measured at the IUCF cooler ring for 104.5 MeV polarized protons is plotted as a function of the longitudinal transverse field error BL in T m. When the spin tune equals to the synchrotron tune beam depolarization was observed. The solid line is obtained from Eqs. (41) and (42) with synchrotron amplitude $\hat{a}=0.001$.

$$S_r\approx-\left[P_{\rm inj}\sin\frac{4G\gamma\pi}{3}\right]\frac{(2-\nu_s)\epsilon}{(2-\nu_s)^2+\epsilon^2}. \tag{40}$$

Thus the effect of a weak solenoidal field error on the spin vector is similar to a single resonance. Varying the solenoidal field is equivalent to varying the resonance strength parameter ϵ.

Now, we include synchrotron sidebands. Since the spin tune at a synchrotron sideband is not an integer, the spin closed orbit associated with the synchrotron sideband precesses about the vertical axis. Only the vertical projection along the closed orbit of the synchrotron sideband can survive.

Combining the stable spin vector of the imperfection resonance and synchrotron sidebands, the final polarization becomes

$$S_v\approx P_{\rm inj}\frac{(2-\nu_s)^2}{(2-\nu_s)^2+\epsilon^2}\frac{(Q_s-\nu_{\rm syn})^2}{(Q_s-\nu_{\rm syn})^2+\epsilon_{\rm syn}^2}, \tag{41}$$

$$S_r\approx-\left[P_{\rm inj}\sin\frac{4G\gamma\pi}{3}\right]\frac{(2-\nu_s)\epsilon}{(2-\nu_s)^2+\epsilon^2}\frac{(Q_s-\nu_{\rm syn})^2}{(Q_s-\nu_{\rm syn})^2+\epsilon_{\rm syn}^2}, \tag{42}$$

where Q_s is the fractional part of the spin tune, $\nu_{\rm syn}$ is the synchrotron tune, and $\epsilon_{\rm syn}$ is the resonance strength of the synchrotron sideband, which can be calculated from Table I. The solid line shown in Fig. 4 is the theoretical fit with a type-3 snake tune shift of $+0.0035$ [19,20] and a synchrotron tune 0.0046 with synchrotron amplitude

$$\hat{a}=\frac{2\nu_{\rm syn}}{|\eta|B_f}\approx0.001,$$

where $|\eta|\approx0.76$ is the phase slip factor, $B_f\approx10$ is the bunching factor. The resulting g is about 0.1. We note that the radial polarization is slightly shifted from the zero crossing point at a fully compensated solenoidal field. In an earlier study [11], we found that the regular imperfection resonance at $\nu_s=2$ with resonance strength of the order of 0.0008 could give rise to a shift and asymmetry in the radial polarization. The solid line has provided a good description of the synchrotron sideband with only a single parameter of synchrotron amplitude $\hat{a}$. Without the kinematic enhancement, the resonance width would have been too small to explain the data.

C. Synchrotron sidebands of rf solenoidal fields

Applying an rf solenoidal field to measure the spin tune of the beam, synchrotron sidebands have also been observed. Using Eq. (2), the resonance strength due to the rf solenoid field is given by

$$\epsilon_K=\frac{(1+G)B_{\|}L}{2\pi B\rho},\quad K=K_{\rm sol}=n\pm\frac{f_{\rm sol}}{f_0}, \tag{43}$$

where $f_{\rm sol}$ is the frequency of the solenoid rf field, and η is an integer. Thus the rf solenoid field generates a resonance at a tune given by the ratio of rf frequency to the revolution frequency.

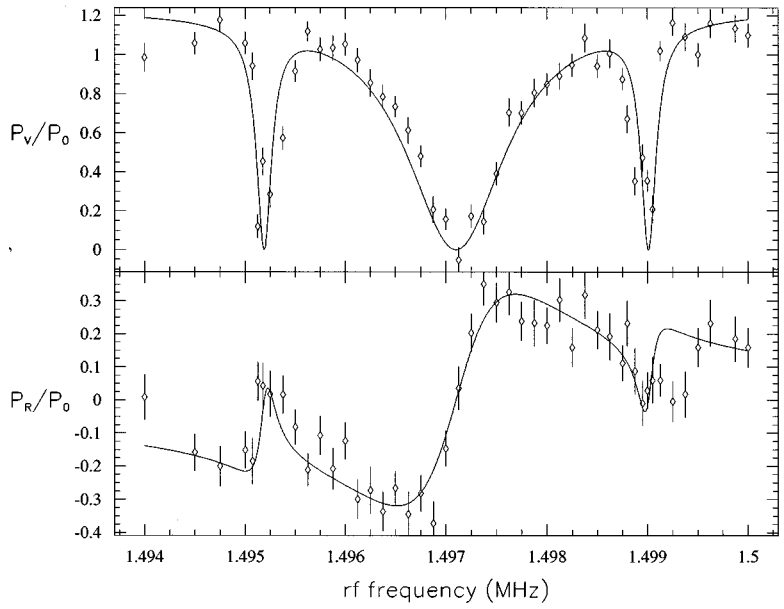

FIG. 5. The vertical (upper plot) and the radial (lower plot) polarizations measured at the IUCF cooler ring are shown as a function of the rf frequency of the rf solenoid. The solid line is obtained from Eqs. (31) and (32) of the nearly overlapping resonance model with the synchrotron amplitude $\hat{a}=0.001$.

Figure 5 shows the vertical and radial polarizations as a function of the rf solenoidal frequency measured at the IUCF cooler ring [12]. The proton beam energy was 104.14 MeV and the revolution frequency was 1.505 MHz. Figure 5 shows particularly that the synchrotron sidebands are important and the radial polarization is not zero.

It is tempting to think that the associated synchrotron sidebands arise from the dependence of $B\rho$ on the momentum, i.e.,

$$B\rho=(B\rho)_0\left(1+\frac{\Delta p}{p_0}\right). \tag{44}$$

Substituting $B\rho$ into Eq. (2), synchrotron sidebands can be generated. However, because $\Delta p/p_0\leqslant 0.001$ is small, the resonance width is simply too small to account for the width observed in Fig. 5.

In the following, we will use the overlapping resonance model with synchrotron sideband enhancement to analyze the data. At 104.14 MeV, we have $G\gamma=1.9918$. Including a type-3 snake tune shift of about $\Delta\nu_3=0.002\,33$ [19], the spin tune was $\nu_s=1.9942$. The rf solenoidal field strength was calibrated to obtain a resonance strength of $\epsilon_K=(4.1\pm 0.2)\times 10^{-4}$. The synchrotron tune was 0.001 271, which gave rise to the parameter $g=(\beta^2 G\gamma_0/\nu_{\rm syn})\hat{a}\approx 0.30$ with the momentum spread about $\hat{a}\approx 0.001$. Thus the effective resonance strengths are about $J_0(g)\epsilon_K\approx 4.0\times 10^{-4}$ for the principle resonance, and $J_1(g)\epsilon_K=6\times 10^{-5}$ for synchrotron sidebands.

Using these parameters, solid lines are obtained from Eqs. (41) and (42) for the vertical and the horizontal polarization, respectively. It is worth noting that the nonzero value of horizontal polarization indicate that the rf solenoid provided an imperfection resonancelike spin resonance to the polarized beam. If $K_{\rm sol}$ is not an integer, the radial polarization will precess about the vertical axis at a frequency $|f_{\rm sol}-f_0|$. The time average will be zero.

The puzzle was resolved by knowing the fact that the rf solenoid used in this experiment acted like a broadband rf system and the beam was actually trapped by the bucket area created by the induced rf electric field. A beam dynamics experiment, performed by the IUCF accelerator physics group, confirmed this explanation. Thus the radial polarization survives for the principle resonance and synchrotron sidebands. At any frequency, the polarized beam particles are trapped into the rf solenoidal bucket. Since $K_{\rm sol}$ was always an integer, the radial polarization at the synchrotron sidebands differs from that of Fig. 4.

V. CONCLUSION

In conclusion, we have discussed the physics of synchrotron sidebands and found that the resonance arises from the kinematic spin phase modulation. Thus the resonance strength is proportional to that of the primary resonance. In the overlapping resonance regime, we find that the overlapping spin resonances can be combined into a single resonance with an effective resonance strength, which depends on the relative phase of each resonance. Using this result, we prove that the effective resonance strength of overlapping synchrotron sidebands for proton synchrotrons is equal to its principle resonance strength with a phase shift. In the case of nearly overlapping spin resonances, we express the polarization vector in terms of spin closed orbits of spin precessing frames. This model is used to analyze polarization data from SPEAR and the IUCF cooler ring. These polarization data are found to be consistent with the model in which synchrotron sidebands are generated by the kinematic effect of spin phase modulation due to synchrotron motion.

ACKNOWLEDGMENTS

We are grateful to Dr. J. Johnson and Professor A. D. Krisch for allowing us to analyze their published and unpublished data. We thank Dr. R. Phelps for his help in providing us the data shown in Fig. 5. This work is supported in part by grants from NSF PHY-9512832 and the U.S.DOE DE-FG02-92ER40747. M. Berglund would like to thank the Blanceflor foundation, Stockholm, Sweden for financial support.

[1] L. H. Thomas, Philos. Mag. **3**, 1 (1927); V. Bargmann, L. Michel, and V. L. Telegdi, Phys. Rev. Lett. **2**, 435 (1959).
[2] E. D. Courant and R. Ruth, BNL Report No. BNL-51270, 1980 (unpublished).
[3] S. Tepikian, S. Y. Lee, and E. D. Courant, Part. Accel. **20**, 1 (1986).
[4] E. D. Courant and H. S. Snyder, Ann. Phys. (N.Y.) **3**, 1 (1958).
[5] S. Y. Lee and S. Tepikian, Phys. Rev. Lett. **56**, 1635 (1986); S. Tepikian, Ph.D. thesis, SUNY Stony Brook, 1988 (unpublished); S. Y. Lee and E. D. Courant, Phys. Rev. D **41**, 292 (1990).
[6] S. Y. Lee, Phys. Rev. E **47**, 3631 (1993).
[7] J. R. Johnson *et al.*, Nucl. Instrum. Methods **204**, 261 (1983).
[8] F. Z. Khiari *et al.*, Phys. Rev. D **39**, 45 (1989); Ph.D. thesis, University of Michigan, 1988 (unpublished).
[9] A. D. Krisch *et al.*, Phys. Rev. Lett. **63**, 1137 (1989).
[10] J. E. Goodwin *et al.*, Phys. Rev. Lett. **64**, 2779 (1990), J. E. Goodwin, Ph.D. thesis, Indiana University, 1990 (unpublished).
[11] M. G. Minty, Ph.D. thesis, Indiana University, 1991 (unpublished); M. G. Minty *et al.*, Phys. Rev. D **44**, R1361 (1991); M. G. Minty and S. Y. Lee, Part. Accel. **41**, 71 (1993).
[12] V. A. Anferov *et al.*, in the 1991-1992 Scientific and Technical Report of IUCF, p. 110 (1992); we thank Prof. A. D. Krisch and his colleagues for allowing us to analyze the unpublished CE20 data used in our analysis; see also Van Guilder, Ph.D. thesis, Michigan University, 1992 (unpublished).
[13] M. Froissart and R. Stora, Nucl. Instrum. Methods **7**, 297 (1960).
[14] A. W. Chao, Nucl. Instrum. Methods **29**, 180 (1981).
[15] S. R. Mane, Nucl. Instrum. Methods **A292**, 52 (1990); *ibid.* **321**, 21 (1992); in *High-Energy Spin Physics*, edited by Kenneth J. Heller, AIP Conf. Proc. No. 187 (AIP, New York, 1989), p. 959.
[16] J. Buon Part. Accel., **32**, 153 (1990), in *High-Energy Spin Physics* (Ref. [15]), p. 963.
[17] The spin chromaticity is defined as $C_s=\gamma(\partial\nu_s/\partial\gamma)$. For a synchrotron without spin rotators $C_s=G\gamma$.
[18] At the IUCF cooler ring, a main solenoid is used to confine cooling electrons. The effect of the main solenoid on the proton beam is compensated locally by two compensating solenoids located just outside the cooling region. The solenoid field used in the experiment was achieved by varying the field of the compensating solenoids.
[19] A pair of toroids, which guide cooling electrons to be mixed with circulating protons, produce a significant vertical closed orbit distortion to the proton beam. To compensate the orbit disturbance, local vertical orbit bumps (with horizontal fields) are used to cancel the toroidal field. The combination of the radial dipole and longitudinal solenoidal fields gives rise to a spin precession around the vertical axis (noncommutativity of Pauli matrices). The resulting spin tune shift was called the type-3 snake [20]. The magnitude of spin tune shift depends on the actual vertical closed orbit and the cooling solenoid field [11]. Thus it can change from one run to the next.
[20] R. Pollock, Nucl. Instrum. Methods A **300**, 210 (1991).